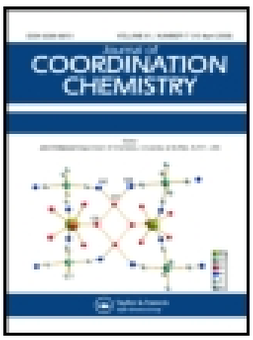

Taylor & Francis
Taylor & Francis Group

Journal of Coordination Chemistry

ISSN: 0095-8972 (Print) 1029-0389 (Online) Journal homepage: http://www.tandfonline.com/loi/gcoo20

Structural conversion of an oxazolidine ligand upon treatment with copper(I) and (II) halides; Structural, spectral, theoretical and docking studies

Zahra Mardani, Vali Golsanamlou, Zahra Jabbarzadeh, Keyvan Moeini, Saba Khodavandegar, Cameron Carpenter-Warren, Alexandra M. Z. Slawin & J. Derek Woollins

To cite this article: Zahra Mardani, Vali Golsanamlou, Zahra Jabbarzadeh, Keyvan Moeini, Saba Khodavandegar, Cameron Carpenter-Warren, Alexandra M. Z. Slawin & J. Derek Woollins (2018): Structural conversion of an oxazolidine ligand upon treatment with copper(I) and (II) halides; Structural, spectral, theoretical and docking studies, Journal of Coordination Chemistry, DOI: 10.1080/00958972.2018.1536268

To link to this article: https://doi.org/10.1080/00958972.2018.1536268

Structural conversion of an oxazolidine ligand upon treatment with copper(I) and (II) halides; Structural, spectral, theoretical and docking studies

ZAHRA MARDANI*†, VALI GOLSANAMLOU†, ZAHRA JABBARZADEH†, KEYVAN MOEINI‡, SABA KHODAVANDEGAR†, CAMERON CARPENTER-WARREN§, ALEXANDRA M. Z. SLAWIN§ and J. DEREK WOOLLINS§

†Inorganic Chemistry Department, Faculty of Chemistry, Urmia University, 57561-51818 Urmia, I. R. Iran
‡Chemistry Department, Payame Noor University, 19395-4697 Tehran, I. R. Iran
§EaStCHEM School of Chemistry, University of St Andrews, St Andrews Fife UK, KY16 9ST

In this work, the 2-(2-(pyridin-2-yl)oxazolidin-3-yl)ethanol (AEPC) ligand was prepared under solvent free conditions using ultrasonic irradiation, before reaction with a $Cu(NO_3)_2$/KSCN mixture, $CuCl_2$ and CuI, the products of which were characterized by elemental analysis, UV-Vis, FT-IR spectroscopy and single-crystal X-ray diffraction. The X-ray analyses results revealed that AEPC, after reactions with the three copper(I/II) halides, gave structures ($[Cu(DEA)Cl_2]$ (**2**), DEA = diethanolamine, $[Cu(BHEG)_2]$ (**3**), BHEG = bis(2-hydroxyethyl)glycinato), however it retains its structure on treatment with $Cu(NO_3)_2$/KSCN mixture ($[Cu(AEPC)(NCS)_2]$ (**1**)). The geometrical parameters for the complexes were compared with the Cambridge Structural Database (CSD) and coordination modes for thiocyanate ion were extracted. In the crystal structure of **1**, the copper ion has a distorted square-pyramidal geometry and a $CuN^{py}N_2{}^{NCS}N^{tert}O^{alc}$ environment in which the AEPC acts as NN'O-donor in a facial coordination mode. In the crystal structure of **2**, the copper ion has a $Cu(N^{sec})(O^{alc})_2Cl_2$ environment and distorted square-pyramidal geometry in which the DEA ligand is coordinated as a *mer*-NO_2-donor. The copper ion in **3** has a CuN_2O_4 environment and distorted octahedral geometry. The ability of these compounds to interact with the nine biomacromolecules (BRAF kinase, CatB, DNA gyrase, HDAC7, rHA, RNR, TrxR, TS and Top II) was investigated by Docking calculations and compared with that of doxorubicin. The thermodynamic stability of **1** and its isomer and also charge distribution patterns were studied by DFT and NBO analysis, respectively.

Keywords: Oxazolidine; Copper halides; DFT Calculations; CSD Studies; Docking studies

*Corresponding author. Email: z.mardani@urmia.ac.ir

1. Introduction

The oxazolidine moiety is an important building block for pharmacologically active compounds such as anti-diabetic [1], anti-tubercular [2], anti-convulsant [3] and aldose reductase inhibitors [4]. It is called pseudo-proline to mimic the proline skeleton for investigation of peptide biological activity [5]. The oxazolidine-based compounds are pseudo-irreversible inhibitors of serine proteases [6] and are used as elastase inhibitors [7]. Some of these derivatives exhibited very high binding affinities for both NK1 and NK2 receptors. There is speculation that a combined NK1 and NK2 receptor antagonist might be an effective drug for the treatment of asthma and chronic airway obstruction [8]. Oxazolidines have been studied extensively as crosslinking agents [9] and for their anti-proliferative activity against cancer cell lines [10].

In order to extend the chemistry of the oxazolidines, we have recently reported two complexes of cadmium and mercury with 2-(2-(pyridin-2-yl)oxazolidin-3-yl)ethanol (AEPC, scheme 1) [11] and in this work, coordination of this ligand to both copper halides and thiocyanate are described. Based on the X-ray analysis, the AEPC ligand converts to the other structures during complexation to the copper(I/II) halides (Cl, I) while keeping its base in treatment with $Cu(NO_3)_2$/KSCN mixture (scheme 2) to produce complexes of $[Cu(AEPC)(NCS)_2]$ (**1**), $[Cu(DEA)Cl_2]$ (**2**), DEA = diethanolamine and $[Cu(BHEG)_2]$ (**3**), BHEG = bis(2-hydroxyethyl)glycinato. In addition to this, synthesis of AEPC by the new optimized method (ultrasonic irradiation) with a higher yield is described, along with the characterization of the compounds and theoretical study of some complexes.

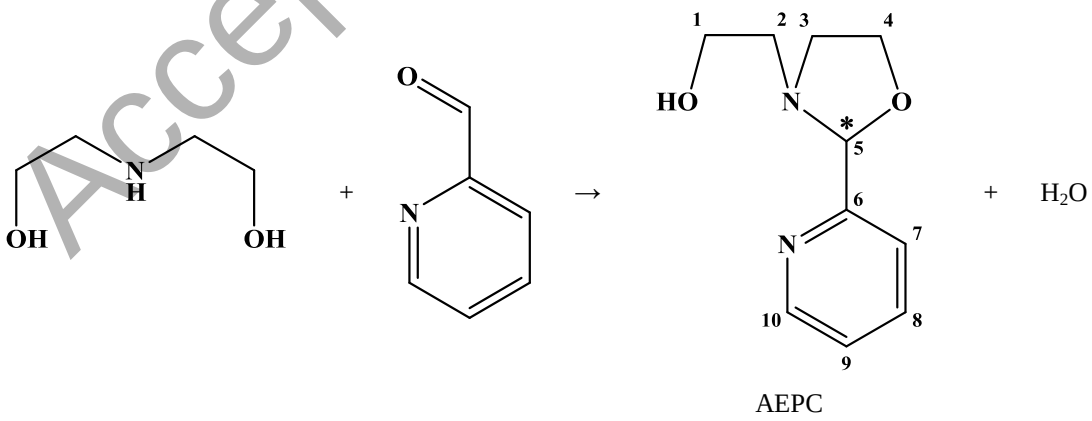

AEPC

Scheme 1. The synthetic route of 2-(2-(pyridin-2-yl)oxazolidin-3-yl)ethanol (AEPC).

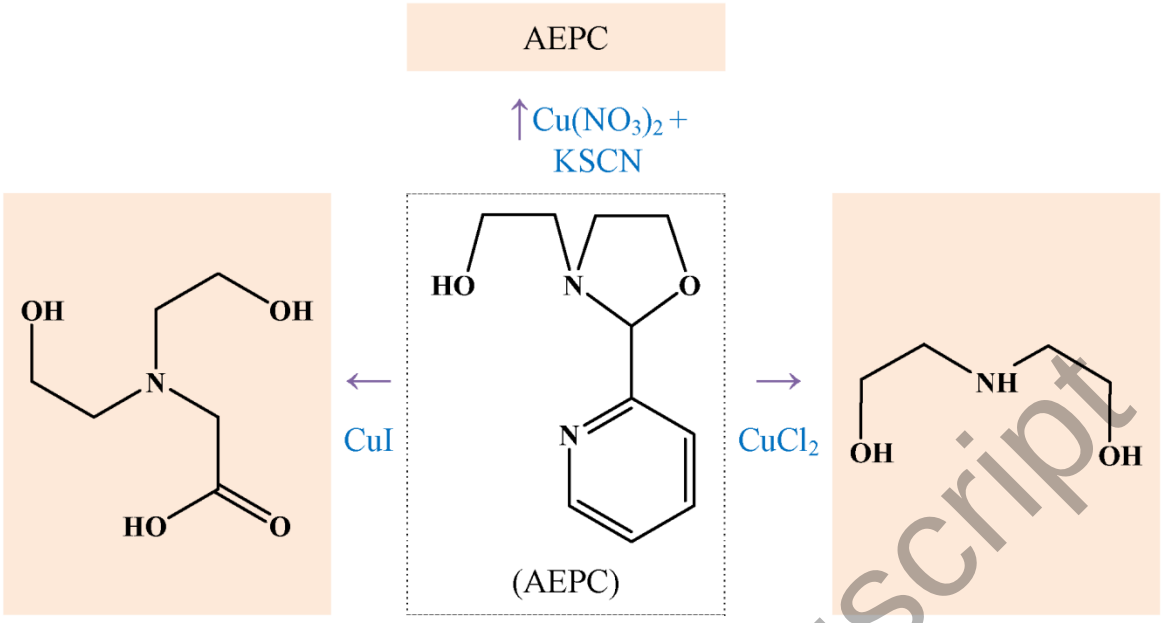

Scheme 2. The structural conversion of the AEPC ligand during complexation process.

In addition to the expected biological properties of AEPC, binding the copper(II) ion to this unit makes these complexes a good choice for biologically active compounds. The copper(II) provides a rapid anti-microbial action without the risk of resistance development [12] and, at the same time, has the ability to modulate angiogenesis, a crucial challenge of current tissue engineering technologies. Moreover, copper(II) is naturally present in the human body, contrary, for instance, to silver [13]. This ion is biocompatible and exhibits many significant roles in biological systems. A further advantage of the copper is that its cost is significantly lower than the therapeutic metals (Pt, Ru, Rh and Au) currently used in the preparation of metal-based anti-cancer agents. A large number of the copper(II) complexes have been reported as potential anti-tumor agents and they have been found to be active both *in vitro* and *in vivo* [14-17].

For predicting the biological activities of the ligand and complexes, docking calculations were run to investigate the possibility of an interaction between these compounds and nine protein targets [18-20], including BRAF kinase, Cathepsin B (CatB), DNA gyrase, Histone deacetylase (HDAC7), recombinant Human albumin (rHA), Ribonucleotide reductases (RNR), Thioredoxin reductase (TrxR), Thymidylate synthase (TS) and Topoisomerase II (Top II). These proteins were selected either due to their reported roles in the cancer growth or as transport agents that affect drug pharmacokinetic properties (*e.g.*, rHA). Also, DNA gyrase was included

to study the possibility of anticancer properties of the compounds, also acting as antimalarial agents [21].

2. Experimental

2.1. *Materials and instrumentation*

All starting chemicals and solvents were from Merck and used as received. Infrared spectra (as KBr pellets) from 4000–400 cm^{-1} were recorded with a FT-IR 8400-Shimadzu spectrophotometer. The carbon, hydrogen and nitrogen contents were determined using a Thermo Finnigan Flash Elemental Analyzer 1112 EA. The melting points were measured with a Barnsted Electrothermal 9200 electrically heated apparatus. The ultrasonic-assisted reaction was carried out using an ultrasonic bath Sonica 2200ETH S3-Soltec. The electronic spectra were recorded in H_2O using a Shimadzu model 2550 UV-Vis spectrophotometer (190–900 nm).

2.1.1. Synthesis of 2-(2-(pyridin-2-yl)oxazolidin-3-yl)ethanol, (AEPC). A mixture of 0.21 g (2 mmol) of 2,2'-azanediylbis(ethan-1-ol) and 0.21 g (2 mmol) of picolinaldehyde was irradiated under reflux condition inside an ultrasonic bath for one hour at 60 °C under solvent-free conditions. After ultrasonic irradiation, a thick brown oil was obtained and the redundant precursors removed by rotary evaporation. Yield: 0.37 g, 95%. Anal. Calcd for $C_{10}H_{14}N_2O_2$ (%): C, 61.84; H, 7.27; N, 14.42. Found: C, 62.13; H, 7.11; N, 14.30. IR (KBr disk): 3363 (ν OH), 3010 (ν CH)$_{ar}$, 2942 (ν CH), 1603 (ν C=N), 1400 (δ_{as} CH_2 and/or ν C=C), 1387 (δ_s CH_2), 1250 (ν C–O), 1040 (ν C–N), 753 and 702 (γ py) cm^{-1}. ^{1}H NMR (300 MHz, [D_6]DMSO): δ = 8.48 (d, 1 H, $C^{10}H$), 7.80 (t, 1 H, C^8H), 7.52–7.55 (d, 1 H, C^7H), 7.32 (m, 1H, C^9H), 4.84 (s, 1H, C^5H), 4.50 (s, 1H, OH), 2.73−3.97 (m, 8H, C^1H_2−C^4H_2) ppm.

2.1.2. Synthesis of (2-(2-(pyridin-2-yl)oxazolidin-3-yl)ethanoldi(thiocyanato)copper(II), [Cu(AEPC)(NCS)$_2$] (1). A solution of 0.19 g (1 mmol) of AEPC, dissolved in ethanol (10 mL), was added to a stirring solution of 0.24 g (1 mmol) of $Cu(NO_3)_2{\cdot}3H_2O$ and 0.29 g (3 mmol) of KSCN in ethanol (10 mL). The reaction mixture was stirred for five days at 60 °C and then filtered. Suitable green crystal prisms for X-ray diffraction studies were obtained by slow evaporation of the solution for four days and collected by filtration. Yield: 0.23 g, 63%; m.p. 299 °C. Anal. Calcd for $C_{24}H_{28}Cu_2N_8O_4S_4$ (%): C, 38.54; H, 3.77; N, 14.98. Found: C, 38.64; H,

3.75; N, 14.90. IR (KBr disk): 3433 w (ν OH), 2173 m and 2066 w (CN^{NCS}), 1608 s (ν C=N)$_{py}$, 1475 w (δ_{as} CH_2), 1384 s (δ_s CH_2), 1293 m (ν C−O), 1054 w (ν C−N), 825 w (ν CS), 767 w and 695 w (γ py) 481 w (δ NCS) cm^{-1}. UV-Vis (H_2O, λ_{max} (nm)/ε): 298/137 (d→d).

2.1.3. Synthesis of dichlorodiethanolaminecopper(II), [Cu(DEA)Cl_2] (2). A solution of 0.19 g (1 mmol) of AEPC, dissolved in ethanol (15 mL), was added to a stirring solution containing 0.17 g (1 mmol) of $CuCl_2 \cdot 2H_2O$ in the same solvent (5 mL). The reaction mixture was stirred for six hours at 50 °C and then filtered. Suitable blue crystal prisms for X-ray diffraction studies were obtained by slow evaporation of the solution for four days and collected by filtration. Yield: 0.1 g, 30%; m.p. 133 °C. Anal. Calcd for $C_4H_{11}Cl_2CuNO_2$ (%): C, 20.05; H, 4.63; N, 5.85. Found: C, 20.18; H, 4.62; N, 5.76. IR (KBr disk): 3389 (ν OH), 3259 (ν NH), 2965 (ν CH), 1463 (δ_{as} CH_2), 1373 (δ_s CH_2), 1235 (ν CO), 1090 (ν CN) cm^{-1}. UV-Vis (H_2O, λ_{max} (nm)/ε): 338/881 (d→d).

2.1.4. Synthesis of bis(bis(2-hydroxyethyl)glycinato)copper(II), [Cu(BHEG)$_2$] (3). A solution of 0.51 g (2.63 mmol) of AEPC, dissolved in ethanol (15 mL), was added to a stirring solution of 0.50 g (2.63 mmol) of CuI in ethanol (5 mL). The reaction mixture was stirred for eight hours at room temperature and then filtered. After a week, the solvent evaporated and an oily compound was obtained. Acetone (15 mL) was added to the resultant oil and stirred for a day before filtration. After evaporation of the acetone, an oily compound formed. By adding distilled water (15 mL) and stirring for one hour and then filtering, the final solution was obtained. The suitable blue crystal prisms for X-ray diffraction studies were obtained by slow evaporation of the solution and collected by filtration. Yield: 0.03 g, 6%; m.p. 203 °C decomposed. Anal. Calcd for $C_{12}H_{24}CuN_2O_8$ (%): C, 37.16; H, 6.24; N, 7.22. Found: C, 37.32; H, 6.31; N, 7.08. IR (KBr disk): 3310 (ν OH), 2946 (ν CH), 1610 (ν_{as} COO), 1405 (ν_s COO), 1463 (δ_{as} CH_2), 1372 (δ_s CH_2), 1242 (ν C−O), 1052 (ν C−N), 665 (δ OCO) cm^{-1}. UV-Vis (H_2O, λ_{max} (nm)/ε): 379/114 (d→d).

2.2. *Crystal structure determination*

X-ray diffraction data for **1** were collected at 93 K using a Rigaku FR-X Ultrahigh Brilliance Microfocus RA generator/confocal optics with XtaLAB P200 diffractometer. Compound **2** was

analyzed at 173 K using a Rigaku SCXmini CCD diffractometer with a SHINE monochromator. Mo Kα radiation (λ = 0.71075 Å) was used and intensity data were collected using ω steps accumulating area detector images spanning at least a hemisphere of reciprocal space. All data were corrected for Lorentz polarization effects. A multiscan absorption correction was applied using CrystalClear [22] or CrysAlisPro [23]. Structures were solved by dual space methods (SHELXT [24]) and refined by full-matrix least-squares against F^2 (SHELXL-2013 [25]). Non-hydrogen atoms were refined anisotropically, and N-H and O-H hydrogen atoms were refined with DFIX restraints, while all other hydrogen atoms were placed geometrically using a riding model. All calculations were performed using the CrystalStructure interface [26]. Selected crystallographic data are presented in table 1. Diagrams of the molecular structure and unit cell were created using Ortep-III [27, 28] and Diamond [29]. Selected bond lengths and angles are displayed in table 2 and hydrogen bond geometries in table 3.

2.3. *Computational details*

All structures were optimized with the Gaussian 09 software [30] and calculated for an isolated molecule using Density Functional Theory (DFT) [31] at the B3LYP/LanL2DZ and B3LYP/6-31+G level of theory for complexes and AEPC, respectively, as well as for NBO analysis. The cif file of **1** and also a similar complex containing an O-donor oxazolidine ligand [32] were used as input files for the theoretical calculations.

2.4. *Docking details*

The pdb files 4r5y, 3ai8, 5cdn, 3c0z, 2bx8, 1peo, 3qfa, 1njb, 4gfh for the nine receptors, BRAF kinase, Cathepsin B (CatB), DNA gyrase, Histone deacetylase (HDAC7), recombinant Human albumin (rHA), Ribonucleotide reductases (RNR), Thioredoxin reductase (TrxR), Thymidylate synthase (TS), and Topoisomerase II (Top II), respectively, used in this research were obtained from the Protein Data Bank (pdb) [33]. The full version of Genetic Optimisation for Ligand Docking (GOLD) 5.5 [34] was used for the docking. The Hermes visualizer in the GOLD Suite was used to further prepare the metal complexes and the receptors for docking. The optimized AEPC ligand and **1** were used for docking calculations. The region of interest used for Gold docking was defined as all the protein residues within the 6 Å of the reference ligand "A" that accompanied the downloaded protein. All free water molecules in the structure of the proteins

were deleted before docking. Default values of all other parameters were used and the complexes were submitted to 10 genetic algorithm runs using the GOLDScore fitness function.

3. Results and discussion

2,2'-Azanediylbis(ethan-1-ol) in the reaction with picolinaldehyde under solvent free conditions using ultrasonic irradiation gave AEPC *via* an oxazolidination reaction (scheme 1). Reaction of AEPC with an ethanolic solution of $Cu(NO_3)_2$/KSCN (1:2) mixture, $CuCl_2$ and CuI in a molar ratio of 1:1 resulted in the formation of **1**-**3**. The complexes are air-stable and soluble in DMSO. Study of the literature revealed that a similar structure to **3** [35-37] has been reported previously from different precursors than those we used. In all CSD searches which have been presented, for more precise results, the structures containing any error or disorder have been omitted.

3.1. *Spectroscopic characterization*

The frequencies of IR bands for the free ligand are different from those of the corresponding complexes providing significant indications of bonding sites of the AEPC. In the IR spectrum of AEPC, a broad peak at 3363 cm^{-1} can be assigned to the *v* (OH) which shifted to higher frequencies in the spectrum of **1** by 70 cm^{-1}, confirming the coordination of an alcohol group to the copper ion. A slight shift (5 cm^{-1}) to higher frequency was observed for the *v*(C=N) of the pyridine ring.

The most interesting part of the spectrum of **1** is the region above 2000 cm^{-1}, where the absorptions due to pseudohalides are observed [38]. Presence of the thiocyanate groups in **1** affects its IR spectrum in three regions: 2000–2200 cm^{-1} for CN stretches, 700–900 cm^{-1} for CS stretches and 400–500 cm^{-1} for SCN bending vibrations [39]. These vibrations can be used to determine the coordination modes of thiocyanato ligands in complexes [38]. In **1**, the peak corresponding to *v*(CN) is split into two peaks, indicating the existence of two non-equivalent coordinated thiocyanate groups and hence mutual *cis* coordination [38, 39]. These peaks appear at 2173 and 2066 cm^{-1} which are higher than those of typical N-bonded thiocyanato (in N-bonded thiocyanato, *v*(CN) appears below 2100 cm^{-1}) [38] which can be attributed to participation of the sulfur atom of the thiocyanato ligand in the hydrogen bonding. The *v*(CS) and *δ*(NCS) in **1** are observed at 825 and 481 cm^{-1}, respectively, which are characteristic frequencies for an N-bonded thiocyanato ligand [38].

In the FT-IR spectrum of **2**, the region above 3000 cm^{-1}, corresponding to the alcohol and amine groups, can be useful for predicting the coordination mode of the DEA ligand. In comparison to the FT-IR spectrum of DEA [39], the *ν*(OH) and *ν*(NH) are shifted about 89 and 59 cm^{-1}, respectively, to higher frequencies than in the free ligand, confirming NO_2-donation of DEA to the copper ion.

In the ^1H NMR spectrum of the ligand (see scheme 1 for numbering), the aromatic hydrogen atoms of the pyridine ring are observed at the lowest magnetic field. Among these protons, $C^{10}H$, which is the closest to the nitrogen atom of the pyridine ring, has the highest ppm value. In the aliphatic region and with increasing the magnetic field, two singlet peaks belonging to the hydrogen atom of the chiral carbon and alcoholic proton are revealed, respectively. The peaks belonging to the other hydrogen atoms of the aliphatic moieties appear in range of 2.7−4.0 ppm.

UV–Vis spectra of the complexes in aqueous solution exhibited a broad absorption attributed to d–d transitions of the copper(II) complexes. The order of energy for the d–d transition is **1** > **2**, showing that the ligand field strength in **1** is higher than in **2**.

3.2. *Description of the crystal structures*

3.2.1. Crystal structure of (2-(2-(pyridin-2-yl)oxazolidin-3-yl)ethanol di(thiocyanato)copper(II), [Cu(AEPC)(NCS)$_2$] (1). In the crystal structure of **1** (figure 1), there are two independent molecules of [Cu(AEPC)$(NCS)_2$] in the asymmetric unit with slightly different geometrical parameters. Each AEPC ligand acts as a tridentate NN'O-donor, with a pyridyl nitrogen donor atom, tertiary amine nitrogen donor atom and alcohol oxygen donor atom, forming two five-membered non-planar chelate rings. The angle between the mean planes through the two chelate rings of the AEPC ligand is 77.12(13) and 73.26(14)°, respectively, for Cu1 and Cu21, showing that the ligand binds to the copper ion in the *fac* formation. A similar coordination manner has been observed for AEPC in reaction with $CdCl_2$ [40]. The C5 carbon atom on the AEPC ligand (scheme 1) has four different substituents and is chiral. In addition to this, a new chiral center is formed (nitrogen atom of oxazolidine ring) upon coordination. Thus each of the two molecules in the asymmetric unit has both a C- and N-chiral centers. The two molecules in the asymmetric unit are different enantiomeric forms of one another, one *R*,*S* and the other *S*,*R*.

The 2-(pyridin-2-yl)oxazolidine unit is potentially a tridentate ligand that can bind to metal ions through one O- and two N- atoms. A survey of the CSD reveals that this unit has two different coordination modes including $N^{py}N^{oxa}$- and $N^{py}O^{oxa}$-donor of which the $N^{py}N^{oxa}$ mode is common. There is only one example for $N^{py}O^{oxa}$-donor mode [32]. The angle between the two mean planes through the pyridine and oxazolidine rings in **1** is 75.94(16) and 74.03(17)°, respectively, for Cu1 and Cu21 proving these rings are almost perpendicular to each other as "face to face" form and the bond angles for chiral carbon atoms in the chelate rings are 111.1(2) and 110.6(2)° for Cu1 and Cu21, respectively (for "face to side" form the bond angle is larger) [11]. The pyridine and oxazolidine rings of the AEPC in the reported cadmium complex have "face to face" direction while in a mercury complex they have "face to side" form [11].

In this structure, the copper ion has a coordination number of five, by coordination of the one oxygen and two nitrogen atoms of one AEPC ligand and two nitrogen atoms of two thiocyanate ions. A five-coordinate geometry of **1** may adopt either a square pyramidal or a trigonal bipyramidal structure which is determined by applying the formula of Addison *et al.* [41, 42]. The angular structural parameters, τ ($\tau = (\beta - \alpha)/60$, where α and β are the two largest angles at the copper ion with $\beta \geq \alpha$), were calculated to be 0.19 and 0.24, respectively, for Cu1 and Cu21, indicating a distorted square-pyramidal geometry for both (figures 1 and 2). In this geometry, the oxygen atom occupies the axial position and four nitrogen atoms lie on the equatorial plane. Among the four copper-nitrogen bond lengths around Cu1, $Cu–N^{NCS}$ (1.944(3) Å, average of two bond lengths) and $Cu–N^{oxa}$ (2.052(3) Å) are the shortest and longest ones. The bond distance of the Cu–O is about 0.169 Å longer than the longest Cu–N, showing the elongated distance along the z-axis. Similar results were observed for the other molecule in the asymmetric unit. A search of the Cambridge Structural Database (CSD) [43] revealed that there are so far no examples of a $CuN^{py}N_2{}^{NCS}N^{tert}O^{alc}$ environment, complex **1** is the first one.

The thiocyanato ligands in **1** coordinate through their nitrogen atom. For studying the different coordination modes of thiocyanate to copper ions, a structural survey using CSD data was carried out and the results are presented in table 4. Based on these data, the terminally N-bonded mode, observed in **1**, is common. The percentage of terminally bonded modes (53%) is slightly higher than the bridging (47%). Interestingly, the thiocyanate ion is also capable of forming a four-membered chelate ring with a copper ion, however this is a very rare mode [44].

Among the bridging modes, bridging NS-donor thiocyanate between two copper ions is more common than any other mode.

For comparing the geometrical parameters of the terminal N-donor coordinated thiocyanato ligands of **1** with the CSD analogues, the bond lengths and angles average for all reported complexes were calculated and presented in scheme 3(a). The results revealed that the N-bonded thiocyanate ligand and copper ion do not form a linear structure (scheme 3(a)). The C−N−Cu angles average and N−Cu bond lengths average in **1** are 172.1° and 1.950 Å, which are higher and lower than the CSD average (scheme 3(a)), respectively. To compare the geometry of the thiocyanate ion in its coordinated and uncoordinated states, a CSD search was performed for free thiocyanate ions (scheme 3(b)). Based on these data, after coordination of thiocyanate the CN and SC bond lengths are slightly increased and decreased, respectively, which is in agreement with the literature for N-bonded thiocyanato ligands [45, 46].

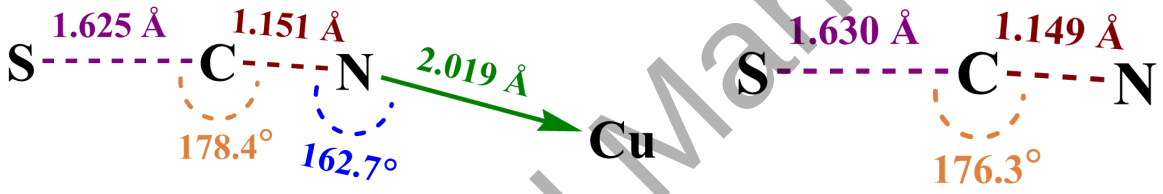

(a) (b)

Scheme 3. (a) The CSD average for geometrical parameters in complexes containing the terminal N-donor thiocyanato ligand. (b) The CSD average for bond lengths and angles for all non-bonded thiocyanate ions.

3.2.2. Crystal structure of dichlorodiethanolaminecopper(II), [Cu(DEA)Cl_2] (2). In the crystal structure of **2** (figure 3), the copper ion is coordinated to one nitrogen and two oxygen atoms of a DEA ligand and two chloride ions, giving a total coordination number of five. The angular structural parameter, τ, was calculated to be 0.40 for the copper ion, indicating a distorted square-pyramidal geometry (figures 3 and 4). In this geometry, the Cl2 ligand occupies the axial position and three donor sites of the DEA along with the Cl1 ligand lie on the equatorial plane. Studying the CSD database revealed that there are no examples of $Cu(N^{sec})(O^{alc})_2Cl_2$ environments that would allow us to compare the geometric parameters with **2**. In another study, all complexes with $CuNO_2Cl_2$ environments (any types of O- and N-donor ligand with terminal

chloride ions) and τ values in the range of 0.00−0.50 (similar as to **2**) were extracted (observed range, 0.04−0.31, three complexes without the equatorial plane were omitted [47-49]). These complexes can be classified in three types (table 5). The (a) type, in which one chloro ligand is located in the axial position, has the largest difference (Δ, table 5) between the bond lengths of the two chloro ligands (the distance of axial Cu−Cl is larger than the equatorial). The mean deviation of the atoms from their equatorial plane is greater in type (a) structures than any of the others. Complex **2** belongs to the (a) type complexes (table 5) with Δ = 0.34 Å and 0.31 Å for the distance of the copper ion from coordinated plane (*d*).

The DEA ligand acts as tridentate NO_2-donor through a secondary amine nitrogen and two alcohol oxygen atoms and forms two five-membered non-planar chelate rings. Each tridentate ligand can coordinate to the metal in facial or meridional forms. In the *mer* form there are two angles of 90° and one at 180°; in the *fac* form there are three angles of 90°. In **2**, two angles of coordinated DEA are deviating from 90° due the chelating bite angle, while the third one is about 149°, confirming *mer* form (135°, exactly half way between *fac* and *mer*) [50, 51].

3.2.3. Crystal network interactions. In the crystal networks of **1** and **2** (figures 2 and 4, respectively) intermolecular O–H···S (**1**) and O–H···Cl (**2**) hydrogen bonds appear between different moieties. In this way the sulfur atom and chloride ion act as proton acceptors and oxygen atoms participate in hydrogen bonding as proton donors and acceptors, simultaneously. In addition to hydrogen bonds, there are short contact interactions between the sulfur atoms of the adjacent thiocyanate ions (**1**).

In the crystal packing of the complexes, the O–H···Cl (**2**) hydrogen bonds participate in the formation of very different hydrogen bond motifs such as $R_2^2(8)$, $R_6^4(20)$, $R_6^5(22)$ and $R_6^6(24)$ [50, 52] between adjacent complexes.

Total intermolecular interaction energies for single molecules of each complex were calculated using Mercury [53] and its CSD-materials tool [33, 54]. For this, the sum of the intermolecular interactions energies in a molecular packing shell containing 100 molecules around the one complexes **1** and **2** were calculated to be −325.60 (complex **1** containing Cu1), −326.07 (complex **1** containing Cu21) and –10.34 kJ/mol (figure 5), respectively, confirming that one molecule of **1** is more stabilized in the solid state by its network interactions than +**2**. Also the interactions of the enantiomer containing Cu21, in **1**, were slightly stronger than its Cu1

enantiomer. In **1**, 90% (Cu1 enantiomer) and 88% (Cu21 enantiomer) of the total energy is corresponding to the interactions with its 14 closest neighboring molecules (figure 5). The interactions between one molecule of **2** with three molecules in the distance range of 6−7 Å increase the energy component of the molecule by +90.63 kJ/mol. Other interactions decrease the energy level of the studied unit in **2**.

3.3. *Theoretical studies of AEPC and 1*

Study of the literature revealed that of the two possible $N^{py}N^{oxa}$- and $N^{py}O^{oxa}$-donor modes for 2-(pyridin-2-yl)oxazolidine-based ligands, the N_2-donor mode is common while other mode is rare [11]. Based on this observation, the energy level for the optimized complex **1** (**1**^{opt}) in which 2-(pyridin-2-yl)oxazolidine unit acts as a $N^{py}N^{oxa}$-donor was compared with a possible isomer containing $N^{py}O^{oxa}$-donor AEPC, [Cu(AEPC)$(NCS)_2$] (**1**'^{opt}, figure 6). Owing to the spatial restriction effects when the oxazolidine ring is coordinated through the oxygen atom, the alcoholic group on the AEPC ligand cannot be coordinated. Thus in **1**'^{opt}, the AEPC acts as a NO-donor while in **1**^{opt} as N_2O-donor. The DFT calculation revealed that the isolated complex **1**^{opt} is about −6.57 Kcal/mol more thermodynamically stable than the **1**'^{opt}, which is in agreement with the solid state result.

For studying the charge distribution before and after complexation, an NBO analysis was done on the free AEPC and **1** (table 6). The results reveal that the calculated charge on the copper ion is about +0.91 and lower than the formal charge (+2), owing to the electron donation of the ligand during complexation. Based on the calculated total charge values, the total charge of the nitrogen, carbon and oxygen atoms in **1** is more negative than that of the free ligand, while the total charge of hydrogen atoms is more positive than in the free ligand. This observation reveals that the hydrogen atoms play an important role in electron donation toward the metal ion, thus decreasing the charge of the copper ion. The nitrogen atoms on the thiocyanato ligands are more negative than those on the AEPC, showing the nitrogen atoms of the thiocyanate ions are more electronegative than the AEPC nitrogen atoms.

In the optimized AEPC, the HOMO is delocalized on the oxazolidine ring and partially on the ethanolic side arm while the LUMO is delocalized on the pyridine ring (table 7). In **1**^{opt}, the HOMO is almost delocalized on the thiocyanato ligands while the LUMO is delocalized on

the pyridine ring of the coordinated AEPC. The metal ion does not have any significant participation in the frontier molecular orbitals (table 7).

Similar to the solid phase results, in the isolated molecule of $\mathbf{1}^{opt}$, the copper ion has a τ value of 0.04 and square-pyramidal geometry. In this structure, the AEPC ligand is coordinated in *fac* form (the angle between two mean planes through the chelate rings of AEPC is 86.25°).

3.4. *Docking studies of AEPC and 1-3*

For predicting the biological activities of AEPC and **1**-**3**, interactions of these compounds with nine macromolecule receptors using Gold [34] docking software were studied. The Gold docking results are reported in terms of the values of fitness which means that the higher the fitness, the better the docked interaction of the compounds [18-21]. The results of the docking presented in this work are the best binding results out of the ten favorites predicted by Gold. Also for evaluation of the calculated fitness values, these scores were compared with those of the famous anti-cancer drug, doxorubicin (a cancer medication that interferes with the growth and spread of cancer cells in the body [55]).

The general features from the Gold docking prediction (table 8) show that all studied structures can be considered as biologically active compounds [18-20]. The best predicted targets for AEPC is HDAC7, while for the studied complexes TrxR is the target. A comparison of the GOLDScore fitness values for the ligand and **1** showed that **1** had a better interaction with the biomacromolecules (except for CatB which exhibited comparable fitness values). A fitness value comparison between **1**-**3** showed the general trend **1** > **3** > **2** in their binding ability towards proteins. The docking results of the interaction between the ligand and the complexes with BRAF kinase protein are shown in figures 7-10, respectively. In addition to the alcohol and amino moieties in the structures of the complexes, the thiocyanato (**1**) and chloro (**2**) ligands participate in hydrogen bonding with proteins (table 9). Data of table 8 revealed that the ligand or complexes or both of them, in some cases (HDAC7, CatB), have comparable fitness values with the doxorubicin in binding toward the studied biomacromolecules, thus we suggest that the anticancer activities of these compounds will be studied.

4. Conclusion

In this work, four complexes of copper(I/II), [Cu(AEPC)$(NCS)_2$] (**1**), AEPC = 2-(2-(pyridin-2-yl)oxazolidin-3-yl)ethanol, [Cu(DEA)Cl_2] (**2**), DEA = diethanolamine, [Cu$(BHEG)_2$] (**3**), BHEG = bis(2-hydroxyethyl)glycinato, were synthesized in a reaction between AEPC with $Cu(NO_3)_2$/KSCN mixture (**1**) and copper(I/II) halides (**2**, **3**). Their spectral (IR, UV-Vis, ^{1}H NMR) and structural (single crystal X-ray diffraction) properties were investigated. These structural analyses revealed that the AEPC ligand can convert to the other structures during the complexation process. In the crystal structure of **1**, the copper ion has a distorted square-pyramidal geometry and $CuN^{py}N_2^{NCS}N^{tert}O^{alc}$ environment, in which AEPC acts as NN'O-donor in the *fac* form and thiocyanto ligands adopts a terminally N-bonded mode, which is the most common mode of coordination among the CSD selected analogues (53%). In the structure of **2**, the AEPC converts to the DEA ligand and coordinates as a *mer*-NO_2-donor to form a distorted square-pyramidal geometry around the copper ion. In the crystal networks of the complexes, the N–H···Cl (**2**) and O–H···Cl (**2**) hydrogen bonds form very different hydrogen bond motifs. The theoretical studies revealed that the optimized copper(II) complex (**1**^{opt}), which has a similar structure to **1**, is thermodynamically more stable than its isomer containing a $N^{py}O^{oxa}$-donor AEPC, [Cu(AEPC)$(NCS)_2$] (**1**'^{opt}). The docking studies revealed that AEPC and **1**, **2** and **3** can interact with the nine biomacromolecules (BRAF kinase, CatB, DNA gyrase, HDAC7, rHA, RNR, TrxR, TS and Top II). Also the best predicted target for the AEPC is HDAC7, while for the other complexes it is TrxR. The order of the binding affinity of the compounds towards studied proteins is determined as **1** > **3** > **2**.

Supplementary data

CCDC 1814322 and 1814321, respectively, for **1** and **3** contain the supplementary crystallographic data for this paper. These data can be obtained free of charge via http://www.ccdc.cam.ac.uk/conts/retrieving.html, or from the Cambridge Crystallographic Data Centre, 12 Union Road, Cambridge CB2 1EZ, UK; Fax: (+44) 1223-336-033; or E-mail: deposit@ccdc.cam.ac.uk.

References

[1] R.L. Dow, B.M. Bechle, T.T. Chou, D.A. Clark, B. Hulin, R.W. Stevenson. *J. Med. Chem.*, **34**, 1538 (1991).

[2] R.S. Goncalves, C.R. Kaiser, M.C. Lourenco, M.V. De Souza, J.L. Wardell, S.M. Wardell, A.D. Da Silva. *Eur. J. Med. Chem.*, **45**, 6095 (2010).

[3] S.L. Shapiro, I.M. Rose, F.C. Testa, E. Roskin, L. Freedman. *J. Am. Chem. Soc.*, **81**, 6498 (1959).

[4] R.C. Schnur, R. Sarges, M.J. Peterson. *J. Med. Chem.*, **25**, 1451 (1982).

[5] G. Tuchscherer, D. Grell, Y. Tatsu, P. Durieux, J. Fernandez-Carneado, B. Hengst, C. Kardinal, S. Feller. *Angew. Chem. Int. Ed.*, **40**, 2844 (2001).

[6] A.B. Santana, S.D. Lucas, L.M. Gonçalves, H.F. Correia, T.A.F. Cardote, R.C. Guedes, J. Iley, R. Moreira. *Bioorg. Med. Chem. Lett.*, **22**, 3993 (2012).

[7] R. Moreira, A.B. Santana, J. Iley, J. Neres, K.T. Douglas, P.N. Horton, M.B. Hursthouse. *J. Med. Chem.*, **48**, 4861 (2005).

[8] T. Nishi, T. Fukazawa, K. Ishibashi, K. Nakajima, Y. Sugioka, Y. Iio, H. Kurata, K. Itoh, O. Mukaiyama, Y. Satoh, T. Yamaguchi. *Bioorg. Med. Chem. Lett.*, **9**, 875 (1999).

[9] H. Chen, Z.-H. Shana. *Int. J. Biol. Macromol.*, **46**, 535 (2010).

[10] S.F. Andrade, B.G. Oliveira, L.C. Pereira, J.P. Ramos, A.R. Joaquim, M. Steppe, E.M. Souza-Fagundes, R.J. Alves. *Eur. J. Med. Chem.*, **138**, 13 (2017).

[11] Z. Mardani, V. Golsanamlou, S. Khodavandegar, K. Moeini, A.M.Z. Slawin, J.D. Woollins. *J. Coord. Chem.*, **71**, 120 (2018).

[12] M. Vincent, P. Hartemann, M. Engels-Deutsch. *Int. J. Hyg. Environ. Health*, **219**, 585 (2016).

[13] H. Xie, Y. Kang. *Curr. Med. Chem.*, **16**, 1304 (2009).

[14] S. Ramakrishnan, V. Rajendiran, M. Palaniandavar, V.S. Periasamy, B.S. Srinag, H. Krishnamurthy, M.A. Akbarsha. *Inorg. Chem.*, **48**, 1309 (2009).

[15] Q. Wang, M. Zhu, L. Lu, C. Yuan, S. Xing, X. Fu. *Dalton Trans.*, **40**, 12926 (2011).

[16] S. J. Tan, Y. K. Yan, P. P. Lee, K. H. Lim. *Future Med. Chem.*, **2**, 1591 (2010).

[17] M. Alagesan, N.S.P. Bhuvanesh, N. Dharmaraj. *Eur. J. Med. Chem.*, **78**, 281 (2014).

[18] F. Marandi, K. Moeini, F. Alizadeh, Z. Mardani, C.K. Quah, W.-S. Loh, J.D. Woollins. *Inorg. Chim. Acta*, **482**, 717 (2018).

[19] F. Marandi, K. Moeini, F. Alizadeh, Z. Mardani, C.K. Quah, W.-S. Loh. *Z. Naturforsch.*, **73b**, 369 (2018).

[20] Z. Mardani, R. Kazemshoar-Duzduzani, K. Moeini, A. Hajabbas-Farshchi, C. Carpenter-Warren, A.M.Z. Slawin, J.D. Woollins. *RSC Adv.*, **8**, 28810 (2018).

[21] A.A. Adeniyi, P.A. Ajibade. *Molecules*, **18**, 3760 (2013).

[22] CrystalClear-SM Expert, v3.1b27. Rigaku Americas, The Woodlands, Texas, USA, and Rigaku Corporation, Tokyo, Japan (2013).

[23] *CrysAlisPro v1.171.38.41. Rigaku Oxford Diffraction, Rigaku Corporation, Oxford, U.K.* (2015).

[24] G. Sheldrick. *Acta Crystallogr.*, **A71**, 3 (2015).

[25] G. Sheldrick. *Acta Crystallogr.*, **C71**, 3 (2015).

[26] *CrystalStructure v4.2. Rigaku Americas, The Woodlands, Texas, USA, and Rigaku Corporation, Tokyo, Japan* (2015).

[27] L.J. Farrugia. *J. Appl. Crystallogr.*, **30**, 565 (1997).

[28] M.N. Burnett, C.K. Johnson, Ortep-III, Report ORNL-6895. Oak Ridge National Laboratory, Oak Ridge, Tennessee, USA (1996).

[29] G. Bergerhof, M. Berndt, K. Brandenburg. *J. Res. Natl. Stand. Technol.*, **101**, 221 (1996).

[30] M.J. Frisch, G.W. Trucks, H.B. Schlegel, G.E. Scuseria, M.A. Robb, J.R. Cheeseman, G. Scalmani, V. Barone, B. Mennucci, G.A. Petersson, H. Nakatsuji, M. Caricato, X. Li, H.P. Hratchian, A. F. Izmaylov, J. Bloino, G. Zheng, J.L. Sonnenberg, M. Hada, M. Ehara, K. Toyota, R. Fukuda, J. Hasegawa, M. Ishida, T. Nakajima, Y. Honda, O. Kitao, H. Nakai, T. Vreven, J.A. Montgomery Jr., J.E. Peralta, F. Ogliaro, M.J. Bearpark, J. Heyd, E.N. Brothers, K.N. Kudin, V.N. Staroverov, R. Kobayashi, J. Normand, K. Raghavachari, A.P. Rendell, J.C. Burant, S.S. Iyengar, J. Tomasi, M. Cossi, N. Rega, N.J. Millam, M. Klene, J.E. Knox, J.B. Cross, V. Bakken, C. Adamo, J. Jaramillo, R. Gomperts, R.E. Stratmann, O. Yazyev, A.J. Austin, R. Cammi, C. Pomelli, J.W. Ochterski, R.L. Martin, K. Morokuma, V.G. Zakrzewski, G.A. Voth, P. Salvador, J.J. Dannenberg, S. Dapprich, A.D. Daniels, Ö. Farkas, J.B. Foresman, J.V. Ortiz, J. Cioslowski, D.J. Fox, *Gaussian 09*, in, Gaussian, Inc., Wallingford, CT, USA (2009).

[31] J.P. Perdew. *Phys. Rev.*, **B33**, 8822 (1986).

[32] G.A. Ardizzoia, S. Brenna, B. Therrien. *Dalton Trans.*, **41**, 783 (2012).

[33] A. Gavezzotti. *Acc. Chem. Res.*, **27**, 309 (1994).

[34] G. Jones, P. Willett, R.C. Glen, A.R. Leach, R. Taylor. *J. Mol. Biol.*, **267**, 727 (1997).

[35] N.N. Anan'eva, I.N. Polyakova, T.N. Polynova, M.A. Porai-Koshits, N.D. Mitrofanova. *J. Struct. Chem.*, **16**, 448 (1975).

[36] H. Thakuria, G. Das. *Polyhedron*, **26**, 149 (2007).

[37] M.K. Ammar, F.B. Amor, A. Driss, T. Jouini. *Z. Kristallogr. - New Cryst. Struct.*, **216**, 665 (2001).

[38] K. Nakamoto, 6th Edn., Infrared and Raman Spectra of Inorganic and Coordination Compounds, John Wiley, Hoboken (2009), pp. 232.

[39] F. Marandi, K. Moeini, A. Rudbari Hadi. *Z. Naturforsch.*, **71b**, 959 (2016).

[40] Z. Mardani, V. Golsanamlou, S. Khodavandegar, K. Moeini, A.M.Z. Slawin, J.D. Woollins. *J. Coord. Chem.*, **71**, 120 (2018).

[41] A.W. Addison, T. Rao, J. Reedjik, J.V. Rijn, G. Verschoor. *Dalton Trans.*, 1349 (1984).

[42] M. Hakimi, Z. Mardani, K. Moeini, F. Mohr. *Polyhedron*, **102**, 569 (2015).

[43] F.H. Allen. *Acta Crystallogr.*, **B58**, 380 (2002).

[44] M. Kabesova, J. Soldanova, M. Dunaj-Jurco. *Proc. Conf. Coord. Chem.*, **10**, 183 (1985).

[45] A. Lalegani, M. Khaledi Sardashti, R. Gajda, K. Woźniak. *J. Mol. Struct.*, **1149**, 777 (2017).

[46] G.L. Miessler, D.A. Tarr, *Inorganic Chemistry*, Upper Saddle River, N.J., Pearson Education (2004), pp. 54.

[47] P.-D. Mao, L.-L. Yan, W.-N. Wu, B.-X. Yao, M.-Q. Liu, Y. Wang. *Wuji Huaxue Xuebao*, **32**, 1476 (2016).

[48] L. Lin, X.-H. Li, B. Zhang, Z.-Y. Zhang, W.-N. Wu, Y. Wang. *Wuji Huaxue Xuebao*, **32**, 1653 (2016).

[49] Z.-L. You, H.-L. Zhu. *Acta Crystallogr.*, **C60**, m445 (2004).

[50] M. Hakimi, Z. Mardani, K. Moeini, F. Mohr, M.A. Fernandes. *Polyhedron*, **67**, 27 (2014).

[51] M. Hakimi, Z. Mardani, K. Moeini, N. Feizi, F. Mohr. *J. Coord. Chem.*, **70**, 1247 (2017).

[52] M. Hakimi, K. Moeini, Z. Mardani, F. Mohr. *Polyhedron*, **70**, 92 (2014).

[53] C.F. Macrae, I.J. Bruno, J.A. Chisholm, P.R. Edgington, P. Mccabe, E. Pidcock, L. Rodriguez-Monge, R. Taylor, J. Van De Streek, P.A. Wood. *J. Appl. Crystallogr.*, **41**, 466 (2008).

[54] A. Gavezzotti, G. Filippini. *J. Phys. Chem.*, **98**, 4831 (1994).

[55] *https://www.drugs.com/mtm/doxorubicin.html*, in, (7/19/2018).

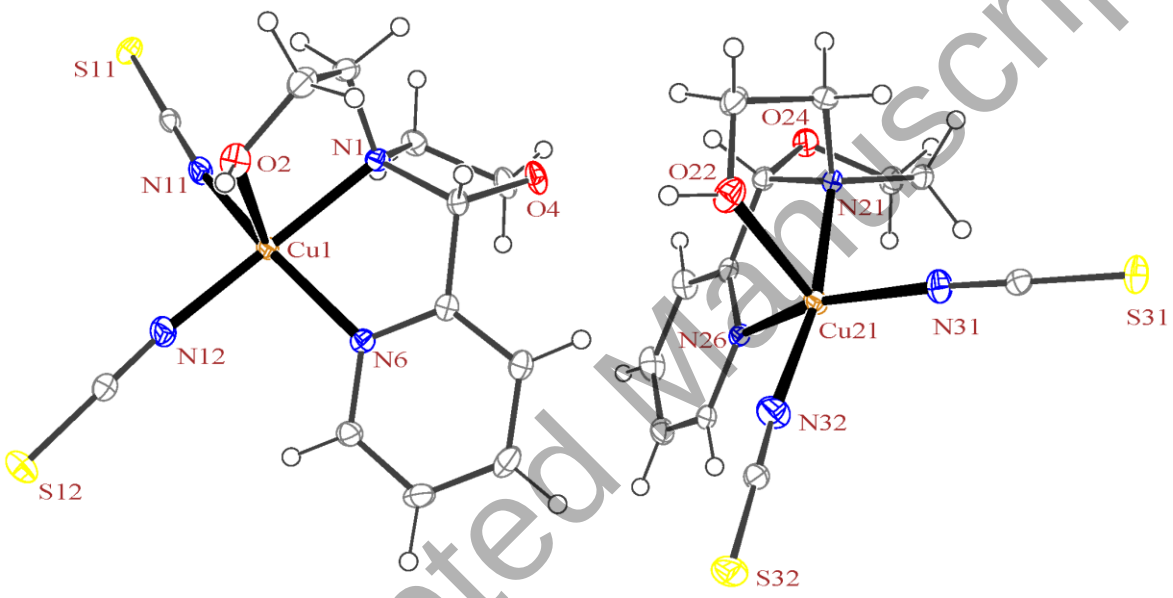

Figure 1. The ORTEP diagram of the molecular structure of **1**. The ellipsoids are drawn at the 35% probability level.

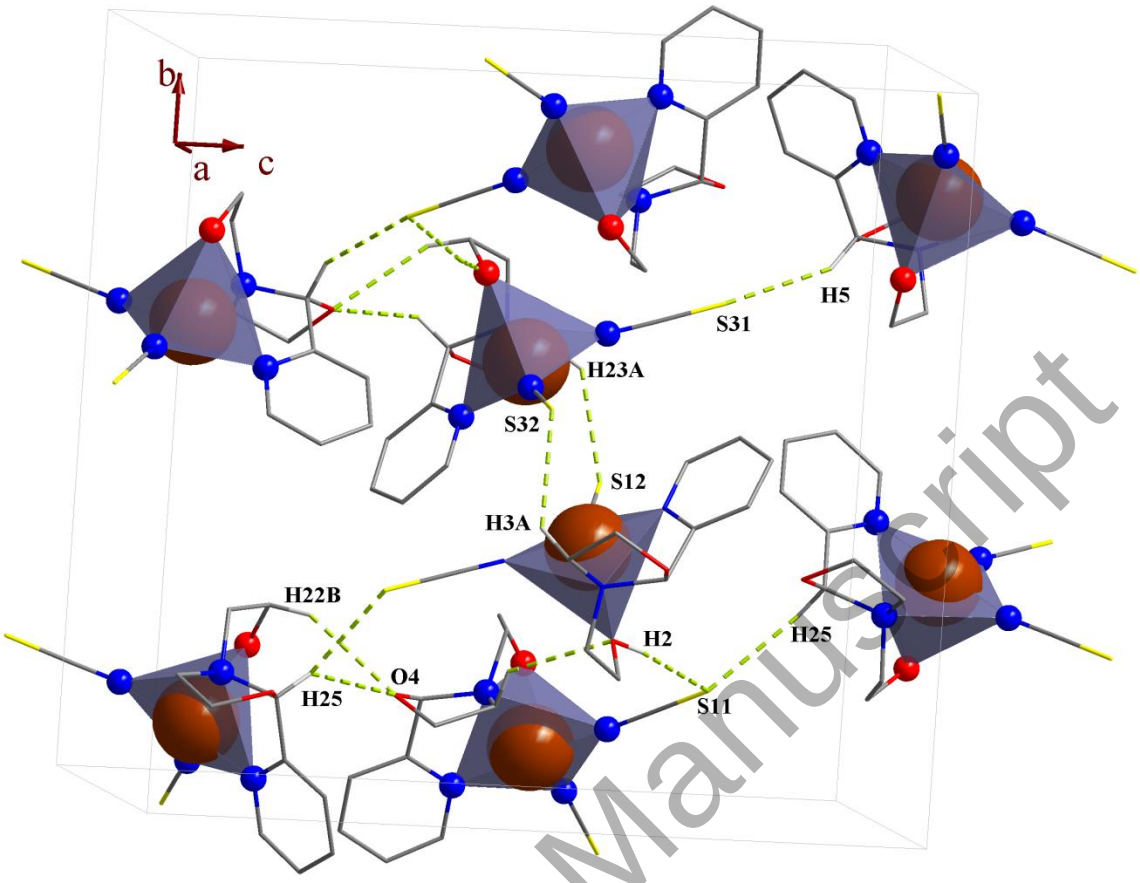

Figure 2. Packing of **1** showing the hydrogen bonds. Only the hydrogen atoms involved in hydrogen bonding are shown. Each CuN_4O unit is shown as square pyramid.

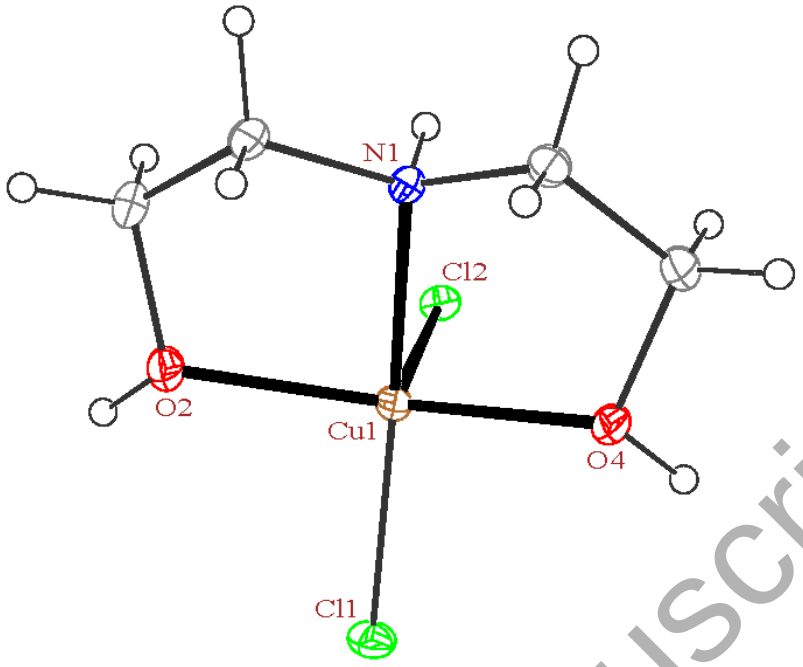

Figure 3. The ORTEP diagram of the molecular structure of **2**. The ellipsoids are drawn at the 35% probability level.

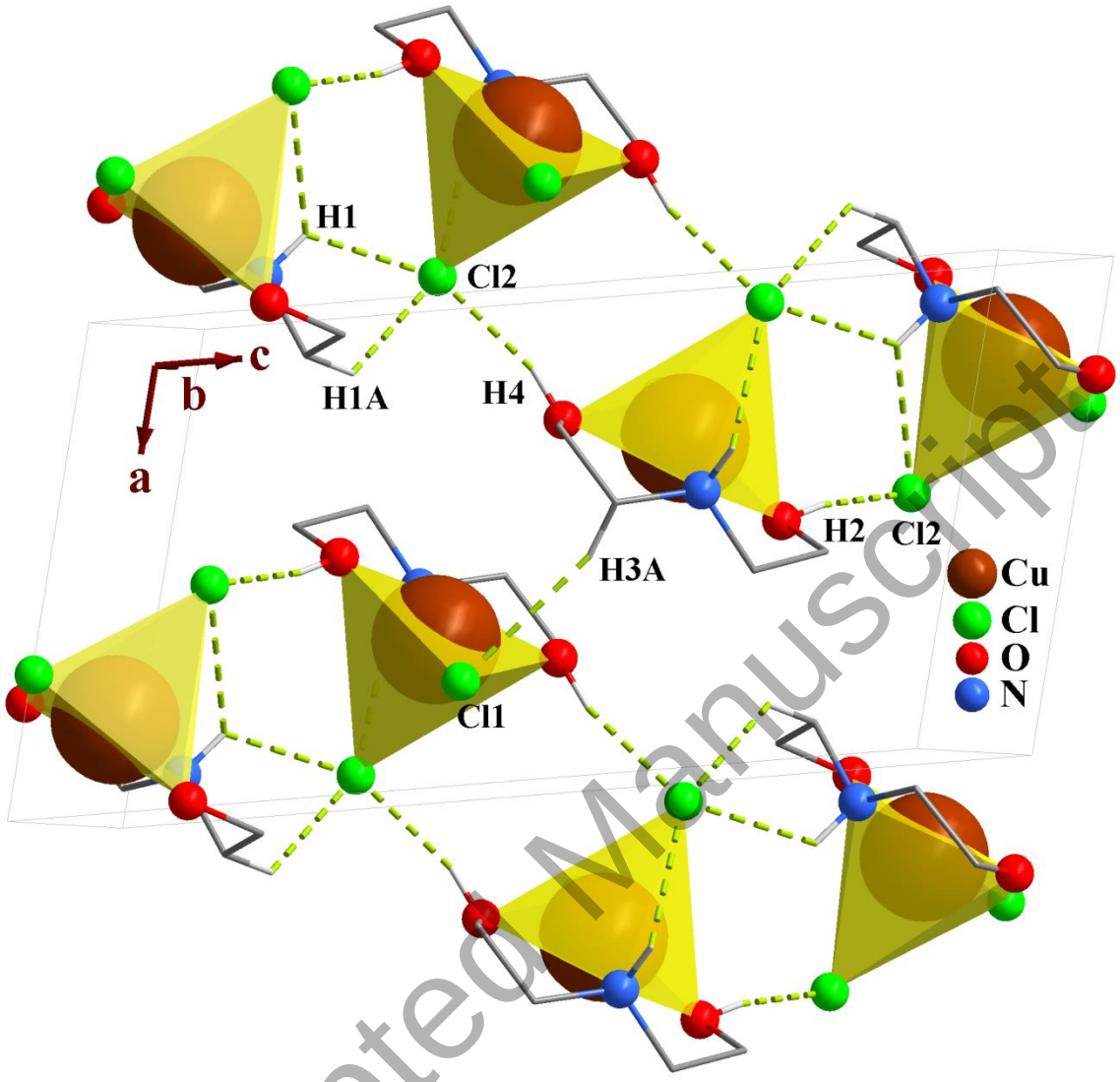

Figure 4. Packing of **2** showing the hydrogen bonds. Only the hydrogen atoms involved in hydrogen bonding are shown. Each $CuNO_2Cl_2$ unit is shown as square pyramid.

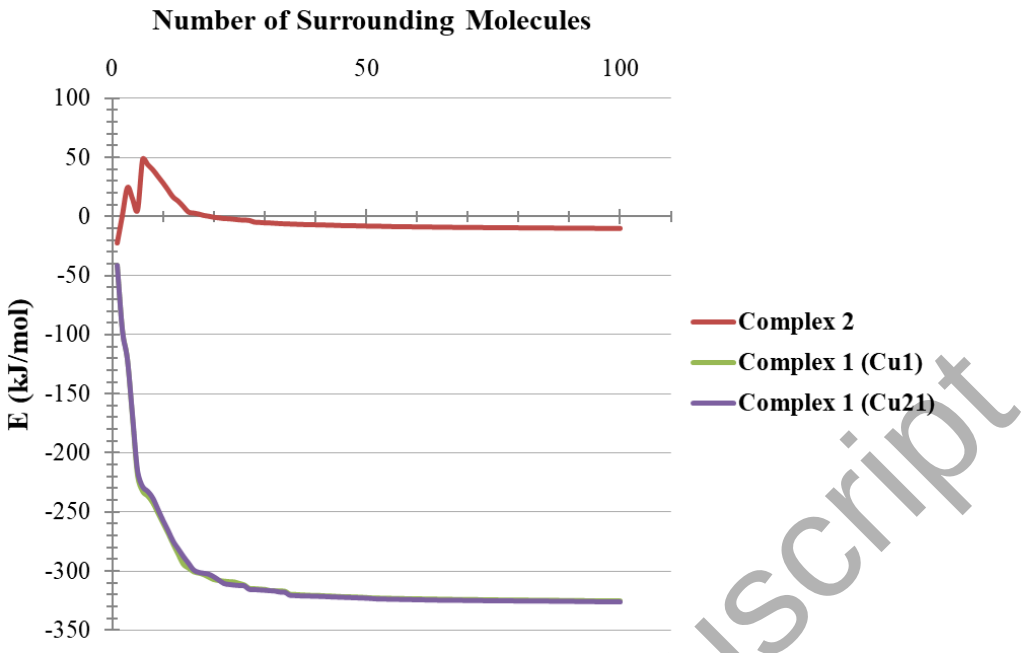

Figure 5. Variation diagram of total intermolecular interactions energy (E) for **1** and **2** with increasing the number of surrounding molecules.

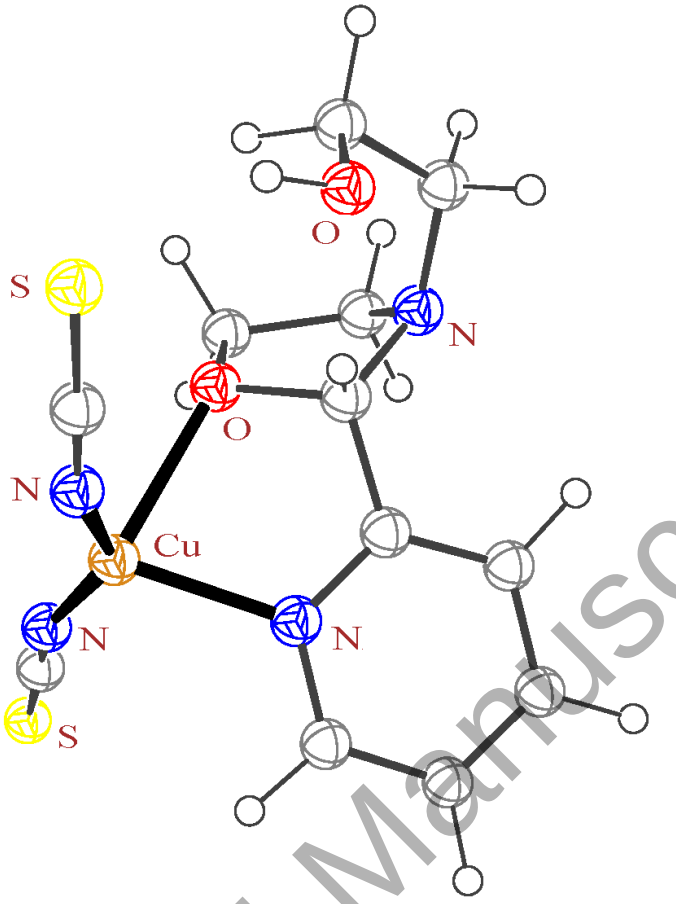

Figure 6. Optimized structure for the complex containing $N^{py}O^{oxa}$-donor AEPC, $[Cu(AEPC)(NCS)_2]$ (**1**'^{opt}), possible isomer for **1**.

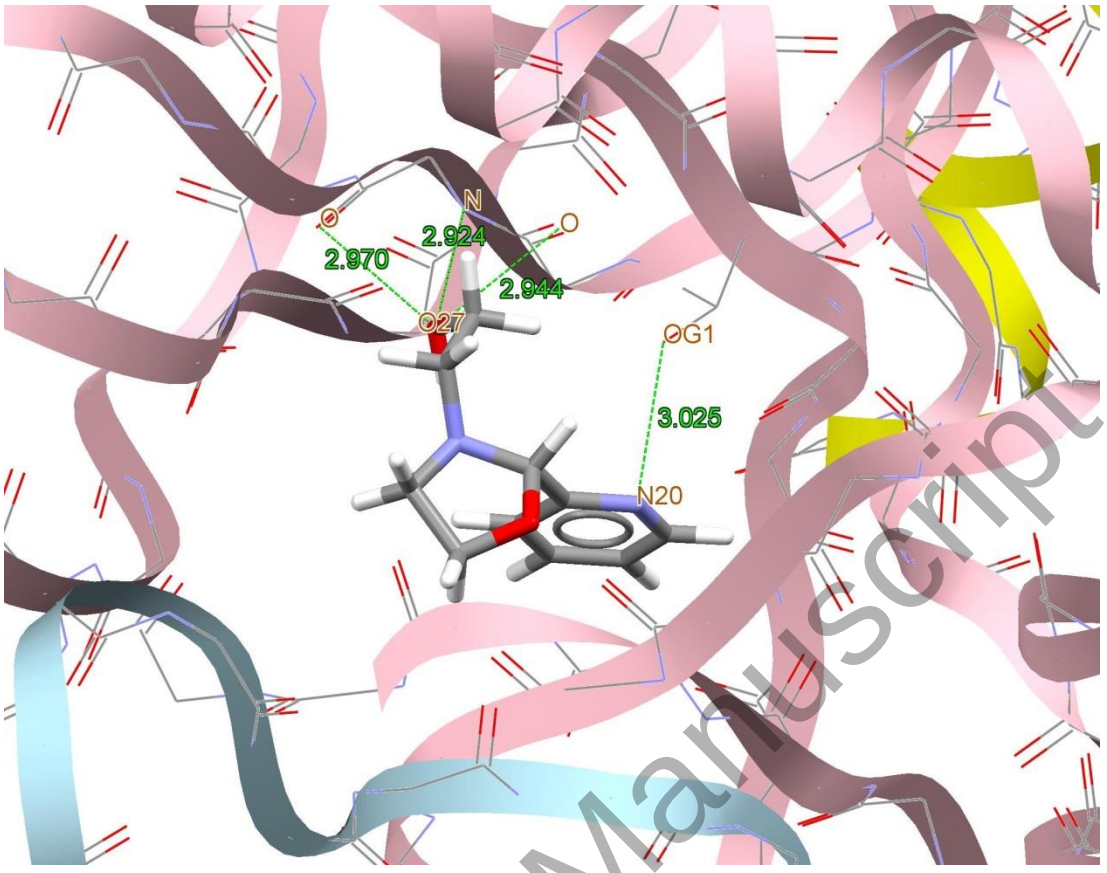

Figure 7. Docking study results showing the interaction between AEPC ligand and BRAF kinase protein.

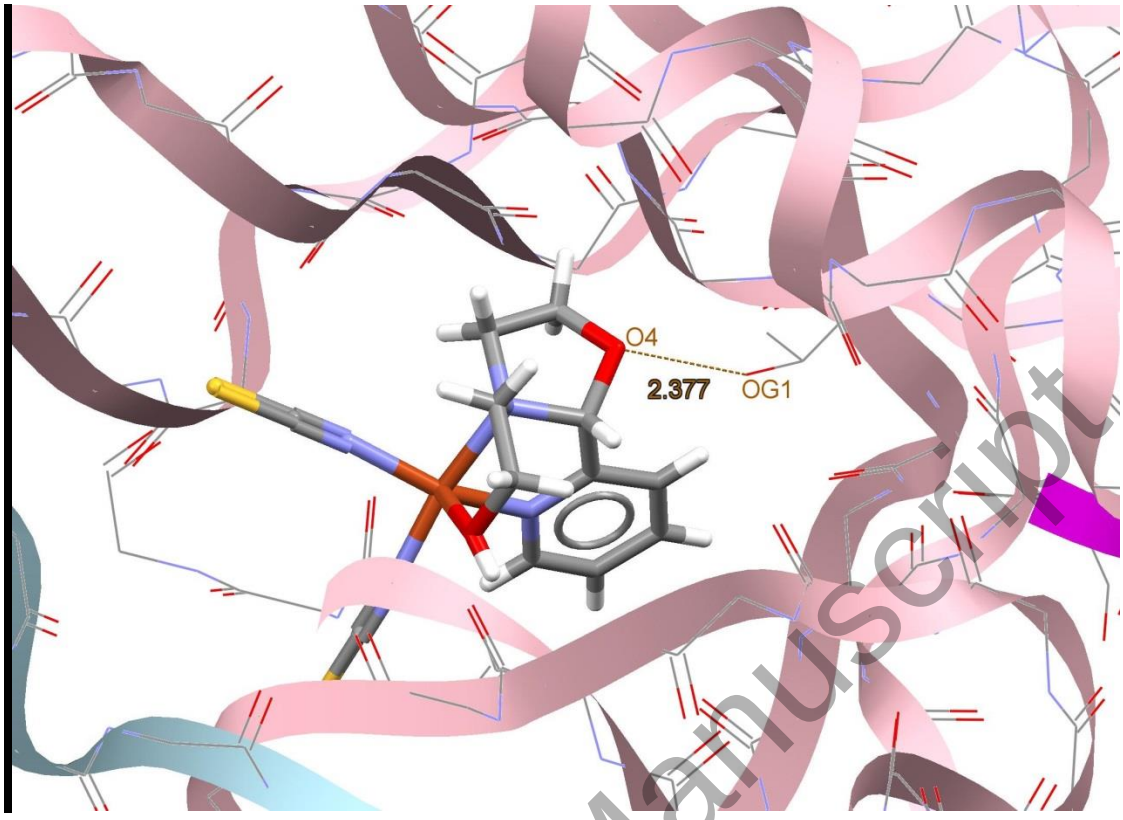

Figure 8. Docking study results showing the interaction between **1** and BRAF kinase protein.

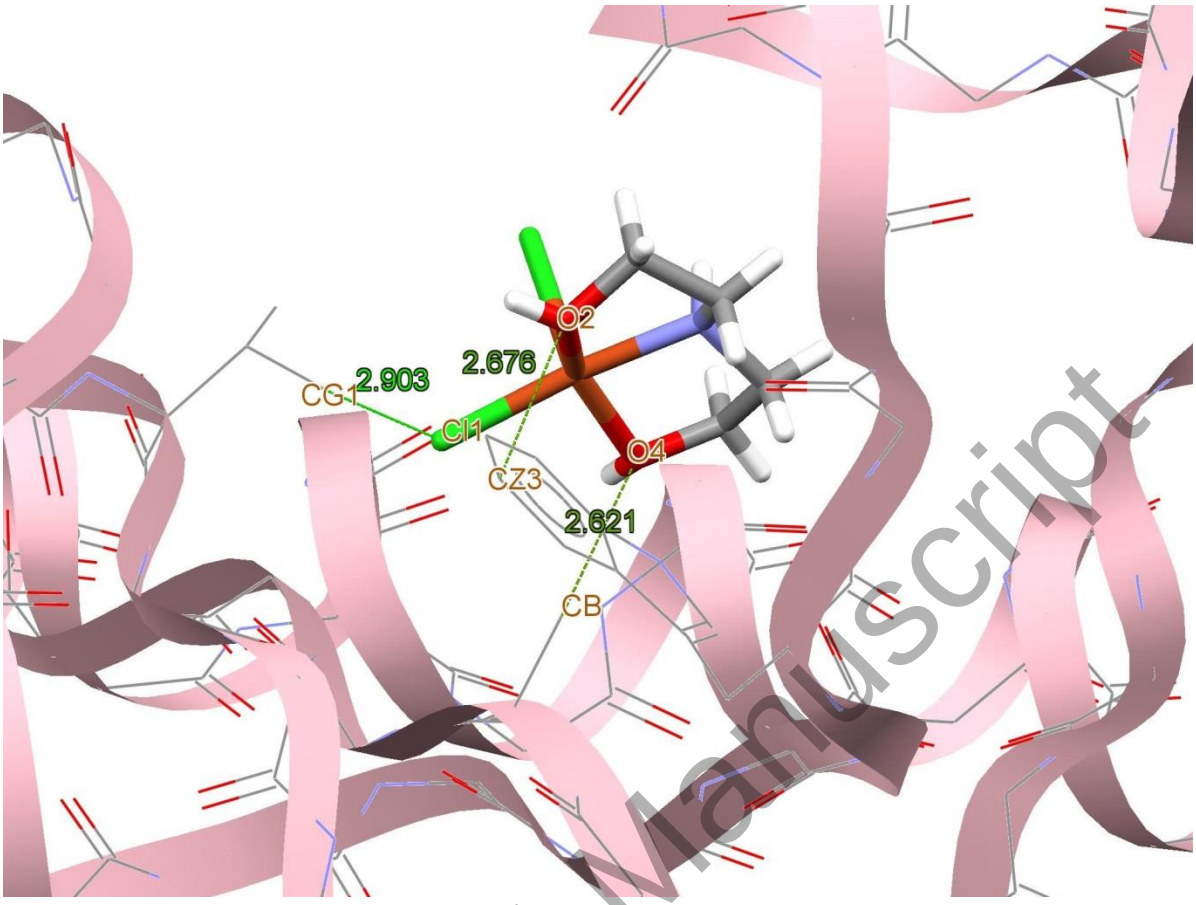

Figure 9. Docking study results showing the interaction between **2** and BRAF kinase protein.

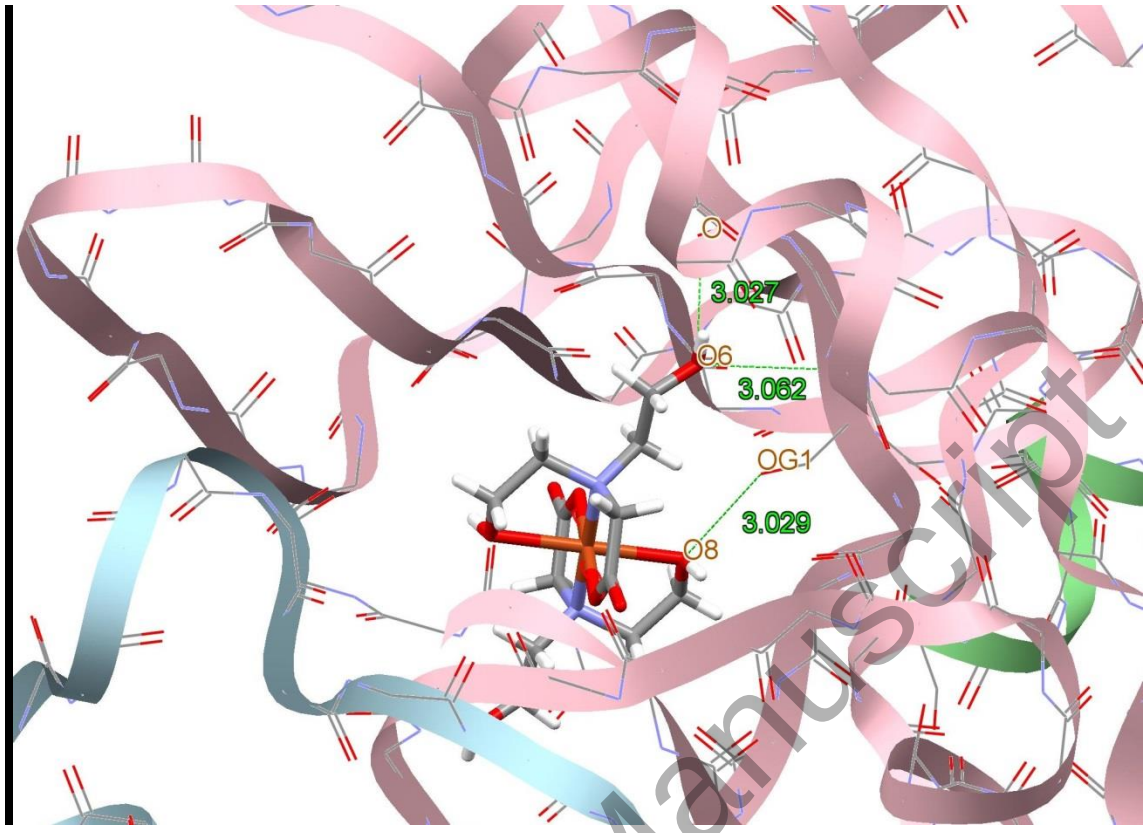

Figure 10. Docking study results showing the interaction between **3** and BRAF kinase protein.

Table 1. Crystal data and structure refinement for **1** and **2**.

	1	**2**
Empirical formula	$C_{24}H_{28}Cu_2N_8O_4S_4$	$C_4H_{11}Cl_2CuNO_2$
Formula weight, g mol^{-1}	747.87	239.59
Crystal size, mm^3	0.12 × 0.12 × 0.09	0.15 × 0.15 × 0.06
Temperature, K	93	173
Crystal system	Orthorhombic	Monoclinic
Space group	$P2_12_12_1$	$P2_1/n$
Unit cell dimensions (Å, °)		
a	9.7908(3)	7.7998(6)
b	17.3016(4)	7.8465(5)
c	18.1819(4)	14.4389(11)
α		
β	90.00	103.817(8)
γ		
Volume, Å^3	3079.95(14)	858.11(11)
Z	4	4
Calculated density, g cm^{-3}	1.613	1.854
Absorption coefficient, mm^{-1}	1.70	3.11
F(000), e	1528	484
2θ range for data collection (°)	4.6–56.4	5.0–63.2
h, k, l ranges	$-11 \le h \le 13$, $-16 \le k \le 21$, $-23 \le l \le 19$	$-11 \le h \le 11$, $-11 \le k \le 11$, $-21 \le l \le 20$
Reflections collected / independent / R_{int}	18136 / 6420 / 0.035	10395 / 2827 / 0.032
Data / ref. parameters	6420 / 383	2827 / 103
Goodness-of-fit on F^2	1.07	1.07
Final R indexes [I>=2σ (I)]	R_1 = 0.026, wR_2 = 0.0650	R_1 = 0.028, wR_2 = 0.0541
Final R indexes [all data]	R_1 = 0.0299, wR_2 = 0.0659	R_1 = 0.0501, wR_2 = 0.0600
Largest diff. peak / hole, e Å^{-3}	0.39 / −0.35	0.46 / –0.38

Table 2. Selected bond length (Å) and angles (°) for **1** and **2** with estimated standard deviations in parentheses.

	1		**2**	
Distances	Cu1−O2	2.277(2)	Cu1−O2	2.0165(13)
	Cu1−N1	2.058(3)	Cu1−O4	2.0189(13)
	Cu1−N6	1.989(3)	Cu1−N1	2.0078(14)
	Cu1−N11	1.962(3)	Cu1−Cl1	2.2122(5)
	Cu1−N12	1.944(3)	Cu1−Cl2	2.5476(5)
	Cu21−O22	2.293(2)		
	Cu21−N21	2.052(3)		
	Cu21−N26	1.994(3)		
	Cu21−N31	1.949(3)		
	Cu21−N32	1.946(3)		
Angles	N1−Cu1−O2	77.83(9)	O2−Cu1−N1	82.54(6)
	O2−Cu1−N11	96.13(10)	N1−Cu1−O4	82.73(6)
	N11−Cu1−N12	94.23(11)	O4−Cu1−Cl1	96.33(4)
	N12−Cu1−N6	93.79(11)	Cl1−Cu1−Cl2	97.068(18)
	N6−Cu1−N1	83.06(10)	Cl2−Cu1−O2	103.37(4)
	N6−Cu1−O2	104.87(10)	N1−Cu1−Cl1	173.06(5)
	N1−Cu1−N12	168.60(12)	O2−Cu1−O4	148.87(6)
	N6−Cu1−N11	157.12(11)		
	N21−Cu21−O22	78.77(9)		
	O22−Cu21−N31	95.24(10)		
	N31−Cu21−N32	94.16(12)		
	N32−Cu21−N26	94.30(11)		
	N21−Cu21−N32	168.60(12)		
	N26−Cu21−N31	154.14(11)		
	N26−Cu21−O22	108.88(10)		
	N26−Cu21−N21	83.12(10)		

Table 3. Hydrogen bond and short contact interactions dimensions (Å and °) in **1** and **2**.

	D–H···A	*d*(D–H)	*d*(H···A)	<(DHA)	*d*(D···A)
1					
	O(2)−H(2)···S(11)	0.90(3)	2.29(3)	172(3)	3.186(3)
	O(22)−H(22)···S(31)	0.93(3)	2.38(3)	169(3)	3.298(3)
2					
	O(2)−H(2)···Cl(2)	0.95(2)	2.09(2)	170(2)	3.0290(14)
	O(4)−H(4)···Cl(2)	0.931(15)	2.171(17)	165.2(18)	3.0801(13)

Table 4. All coordination modes of the thiocyanato ligand with copper ion.

Terminally coordination modes (53%)	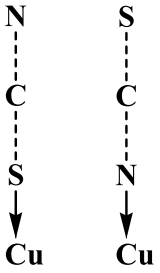		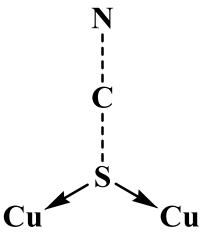	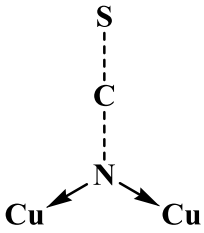	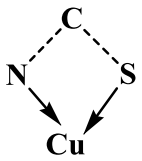
Percent	3.1%	48.1%	0.6%	1.4%	0.1%
Bridging coordination modes (47%)			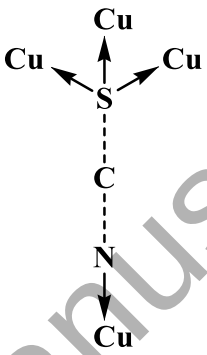	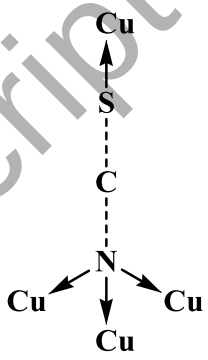	
Percent	36.8%		9.4%	0.3%	0.1%

Table 5. All complexes with $CuNO_2Cl_2$ environment (any types of O- and N-donor ligand with terminal chloride ions) and τ value in range of 0.00−0.50. The Δ value refers to the difference between bond lengths of two chloro ligands and *d* refers to the distance of the copper ion from coordinated plane.

Structures	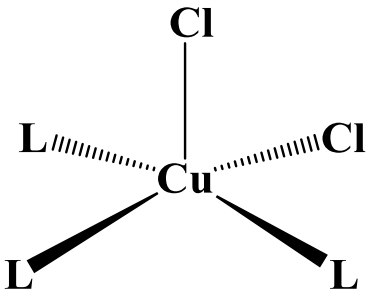	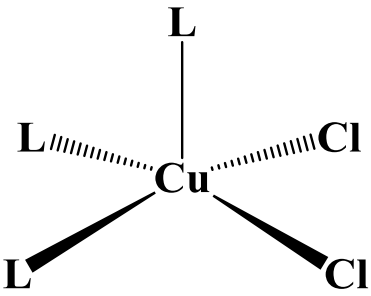	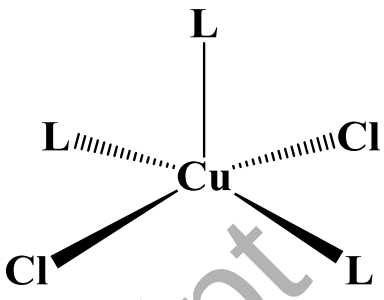
Δ	0.30 Å	0.06 Å	0.03 Å
d	0.30 Å	0.16 Å	0.20 Å
	(a)	(b)	(c)

Table 6. The NBO analysis results for AEPC ligand and **1**^{opt} isolated complex. The values are the total of charge on the similar atoms. The Δ show the variation of charge on the atoms after coordination.

	Carbon	Hydrogen	Nitrogen	Oxygen	S^{NCS}	C^{NCS}	N^{NCS}	Metal
AEPC	–0.52	2.97	–1.09	–1.36	–	–	–	–
1^{opt}	–0.57	3.49	–1.15	–1.39	–0.24	0.35	–1.41	0.91
Δ	–0.05	+0.52	–0.06	–0.03	–	–	–	–

Table 7. HOHO and LUMO orbitals for the optimized structures of AEPC and **1**[opt].

	HOMO	LUMO	Total energy (Kcal/mol)
AEPC	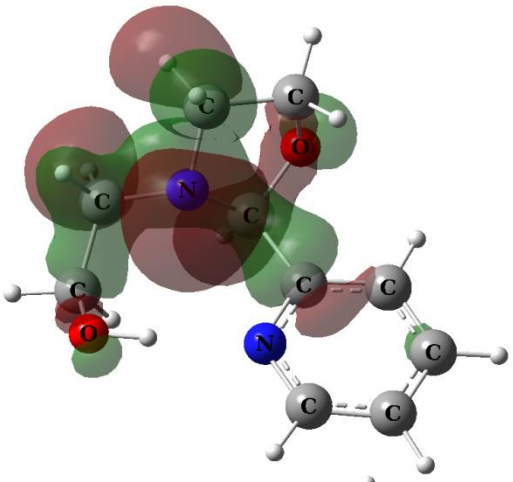	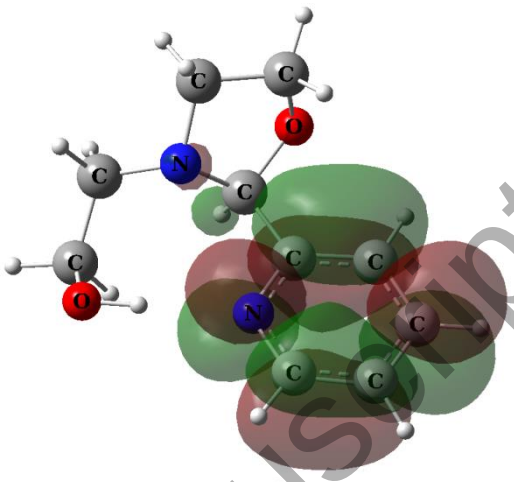	−407620
[Cu(AEPC)(NCS)$_2$]^{Opt} (**1**^{Opt})	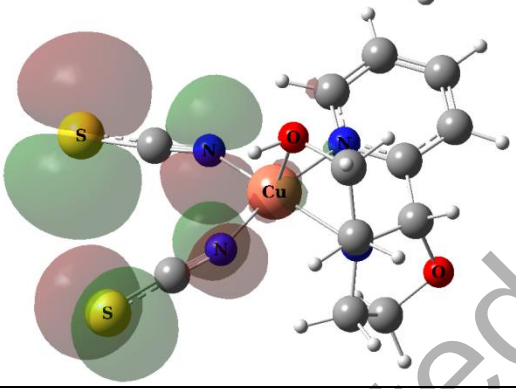	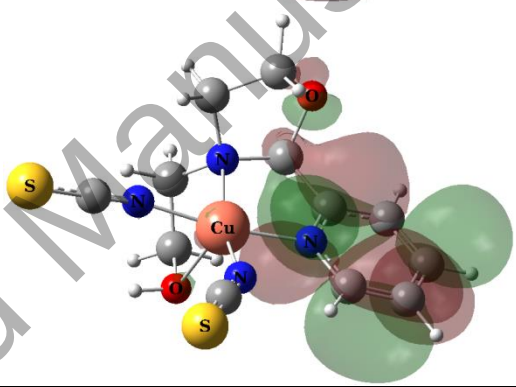	−659766

Table 8. The calculated fitness values for AEPC and **1**-**3** along with the doxorubicin.

	BRAF-Kinase	CatB	DNA-Gyrase	HDAC7	rHA	RNR	TrxR	TS	Top II
AEPC	33.71	26.71	32.68	41.43	34.96	31.76	38.50	35.41	35.49
$[Cu(AEPC)(NCS)_2]$ (**1**)	41.79	26.65	38.09	50.25	43.08	42.55	51.90	48.41	45.46
$[Cu(DEA)Cl_2]$ (**2**)	25.70	15.66	22.59	30.53	26.89	25.95	30.65	27.02	25.04
$[Cu(BHEG)_2]$ (**3**)	40.72	24.36	34.58	33.77	41.01	36.78	46.05	34.10	40.72
Doxorubicin	54.21	25.95	52.97	50.73	50.10	49.18	66.70	53.34	59.05

Table 9. Hydrogen bonds dimensions (Å and °) between proteins and **1**-**3**.

Proteins	D–H···A	*d*(D···A)	Compounds
BRAF-Kinase	O–H^{AEPC}···O	2.944	AEPC
	O–H^{AEPC}···O	2.970	
	N–H···O^{AEPC}	2.924	
	O–H···N^{AEPC}	3.025	
	O–H···O^{1}	2.377	**1**
	C–H···O^{2}	2.621	
	C–H···Cl^{2}	2.903	**2**
	C–H···O^{2}	2.676	
	O–H^{4}···O	3.027	
	N–H···O^{4}	3.062	**3**
	O–H^{4}···O	2.455	
	O–H^{4}···O	3.029	
CatB	C–H···π^{AEPC}	2.865	AEPC
	N–H···O^{1}	2.773	**1**
	N–H···Cl^{2}	2.739	**2**
	N–H···O^{4}	2.426	
	O–H^{4}···O	2.722	**3**
	O–H···O^{4}	2.610	
	O–H···O^{4}	2.426	
DNA-Gyrase	N–H···N^{AEPC}	2.681	AEPC
	O–H^{1}···N	2.819	**1**
	N–H···O^{1}	2.705	
	N–H···Cl^{2}	2.916	**2**
	N–H···Cl^{2}	2.584	
	N–H···O^{4}	2.757	
	O–H···O^{4}	2.506	**3**
	O–H^{4}···O	2.842	
HDAC7	O–H···O^{AEPC}	2.769	AEPC
	C–H···S^{1}	2.759	**1**
	N–H···Cl^{2}	3.200	**2**
	N–H···Cl^{2}	3.063	
	N–H···O^{4}	2.324	
	N–H···O^{4}	2.407	**3**
	O–H^{4}···N	2.826	
rHA	O–H^{AEPC}···O	2.850	AEPC
	O–H···O^{1}	2.588	**1**
	N–H···O^{1}	2.603	
	N–H···O^{1}	2.591	**2**
	N–H···O^{4}	2.804	
	O–H···O^{4}	2.548	**3**
	O–H^{4}···N	2.963	
	O–H^{4}···O	2.753	
RNR	N–H···O^{AEPC}	2.937	AEPC
	O–H···N^{AEPC}	2.797	
	N–H···N^{AEPC}	2.770	
	N–H···O^{AEPC}	2.647	
	O–H^{1}···O	2.569	**1**
	N–H···O^{1}	2.839	
	N–H^{2}···O	3.052	**2**
	N–H···O^{4}	2.512	
	O–H···O^{4}	2.584	
	O–H^{4}···O	2.979	**3**
	N–H···O^{4}	2.660	
	N–H···O^{4}	3.056	
TrxR	O–H···O^{AEPC}	2.974	AEPC
	N–H···N^{AEPC}	2.898	
	N–H···O^{1}	2.172	
	N–H···O^{1}	2.258	**1**
	O–H^{1}···O	2.731	
	O–H^{2}···O	2.927	
	O–H^{2}···O	2.952	**2**
	O–H^{2}···O	3.038	
	N–H···Cl^{2}	2.825	
	O–H^{4}···O	2.702	**3**
	N–H···O^{4}	2.610	
TS	N–H···N^{AEPC}	2.492	AEPC
	S–H···O^{AEPC}	3.107	
	O–H···S^{1}	2.752	**1**
	O–H···O^{2}	2.458	**2**
	N–H···O^{4}	2.797	
	O–H^{4}···O	2.952	**3**
	O–H^{4}···O	2.918	
Top II	N–H···O^{AEPC}	2.690	AEPC
	O–H^{AEPC}···O	2.585	
	O–H^{AEPC}···O	2.552	
	N–H···O^{1}	2.922	
	N–H···O^{1}	2.935	**1**
	O–H^{1}···O	3.026	
	O–H^{2}···O	2.724	
	N–H···Cl^{2}	3.280	**2**
	N–H···Cl^{2}	3.174	
	N–H···Cl^{2}	3.137	
	N–H···O^{4}	3.049	
	O–H···O^{4}	2.336	**3**
	O–H^{4}···O	2.927	
	N–H···O^{4}	2.530